nature communications

Article

https://doi.org/10.1038/s41467-024-50819-7

Nano-anticoagulant based on carrier-free low molecular weight heparin and octadecylamine with an albumin shuttling effect

Received: 1 September 2023

Accepted: 23 July 2024

Published online: 08 August 2024

Check for updates

Jae-Hyeon Lee[1,2,7], Hansol Lim[2,7], Gaeun Ma[2], Seho Kweon[3,4] ✉, Seong Jin Park[5], Minho Seo[1,2], Jun-Hyuck Lee[2], Seong-Bin Yang[2], Han-Gil Jeong[6] & Jooho Park[1,2] ✉

Low-molecular-weight heparin (LMWH), derived from unfractionated heparin (UFH), has enhanced anticoagulant efficacy, long duration of action, and extended half-life. Patients receiving LMWH for preventive therapies would strongly benefit from its long-term effects, however, achieving this is challenging. Here, we design and evaluate a nanoengineered LMWH and octadecylamine conjugate (LMHO) that can act for a long time while maintaining close to 97 ± 3% of LMWH activity via end-specific conjugation of the reducing end of LMWH. LMHO can self-assemble into nanoparticles with an average size of 105 ± 1.7 nm in water without any nanocarrier and can be combined with serum albumin, resulting in a lipid-based albumin shuttling effect. Such molecules can circulate in the bloodstream for 4–5 days. We corroborate the self-assembly capability of LMHO and its interaction with albumin through molecular dynamics (MD) simulations and transmission electron microscopy (TEM) analysis. This innovative approach to carrier-free polysaccharide delivery, enhanced by nanoengineered albumin shuttling, represents a promising platform to address limitations in conventional therapies.

Various polysaccharides are utilized for therapeutic purposes, among which heparin is the most widely used biomolecule that is safe for patients. Heparin is a well-established, FDA-approved anticoagulant drug that has been clinically used for approximately 100 years[1,2]. Despite the advent of direct oral anticoagulants such as rivaroxaban, heparin and its derivatives remain among the most widely used anticoagulant drugs in clinical practice[3,4]. Unfractionated heparin (UFH) has a short half-life (1.5 h)[5] and requires continuous intravenous (I.V.) injection to maintain therapeutic levels, but low-molecular-weight heparin (LMWH) has a longer half-life (2 to 7 h)[5], predictable effect, and minimal side effects, and it can be administered once or twice daily subcutaneously (S.C.), offering more convenient dosing[6]. LMWH has been widely adopted in the clinical management of venous thromboembolism (VTE), deep vein thrombosis (DVT), and pulmonary embolism (PE), demonstrating remarkable efficacy in preventing blood clots[7]. Currently, the global market size of LMWH, estimated at

[1]Department of Biomedical Chemistry, College of Biomedical and Health Science, Konkuk University, Seoul, Republic of Korea. [2]Department of Applied Life Science, BK21 Program, Konkuk University, Chungju, Republic of Korea. [3]Department of Molecular Medicine and Biopharmaceutical Science, Graduate School of Convergence Science and Technology, Seoul National University, Seoul, Republic of Korea. [4]College of Pharmacy, Chonnam National University, Gwangju, Republic of Korea. [5]College of Pharmacy, Seoul National University, Seoul, Republic of Korea. [6]Division of Neurocritical Care, Department of Neurosurgery and Neurology, Seoul National University Bundang Hospital, Seoul National University College of Medicine, Seongnam-si, Republic of Korea. [7]These authors contributed equally: Jae-Hyeon Lee, Hansol Lim. ✉e-mail: seho.kweon@chonnam.ac.kr; pkjhdn@kku.ac.kr

USD 3903 million in 2022, is growing and is expected to reach USD 5733 million by 2028[8].

When using LMWH as anticoagulant therapy, patient compliance with long-term anticoagulant therapy has been limited, because even with the improvements compared to UFH, the route of administration is uncomfortable, and the half-life is still considered short by many patients. There are more than eight FDA-approved LMWHs in the clinical market, and each LMWH displays its own pharmacokinetic (PK) and pharmacodynamic (PD) profiles, with an overall half-life of approximately 3–5 h[9]. In an effort to improve the PK profile of LMWH, fondaparinux was developed as a very low-molecular-weight heparin (VLMWH) with a half-life of 20 h[10]. Despite the clinical importance of heparin, no effective long-acting heparin, i.e., with an action time of more than one day, has been developed so far. A lot of research on increasing the duration of heparin by reducing its molecular size has been conducted, but there are technical limitations because heparin loses its anticoagulant activity when its molecular size becomes too small, i.e., a total size smaller than a pentasaccharide[11–13]. A method for the molecular modification of several carboxyl groups of the heparin structure can be used to increase the action time of the heparin molecules, but a loss of the carboxyl group by chemical conjugation leads to a decrease in their anticoagulant effect[14–16].

Recently, advanced drug delivery systems such as using either functional nanoparticles or endogenous albumin have gained attention for increasing the action time of drugs in the body during therapy[17,18]. Despite the attempts to develop nano-sized, long-acting heparins[19,20], encapsulating heparin molecules within nanoparticles have shown difficult due to their excessive size (>4 kDa), excessive flexibility and strong negative charge. On the other hand, various heparin-based nanoparticles (e.g., heparin/protamine or heparin/chitosan nanocomplexes) without their anticoagulant effect are mainly used for other functions such as eliciting an anticancer effect[21]. The other effective strategy for the continuous delivery of drugs in the bloodstream is to utilize albumin or globulin, which are abundant proteins in the body[22]. In the context of drug delivery strategies, the albumin binding system enhances the PK of biomolecules with otherwise rapid clearance, thereby increasing the efficacy, safety, and usability of DNA, RNA, or peptide-based macromolecules[23–26]. This results in an extended half-life due to low enzyme degradation and elimination resulting from reduced clearance in the kidney, improving their stability in the blood[27,28]. Currently, there are three major methods for inducing interaction with albumin, which are using either a maleimide group, an albumin-binding peptide, or a lipid (fatty acid) group[29]. Of these, fatty acids such as medium-chain or long-chain fatty acids can bind to human serum albumin (HSA) with high affinity at multiple (around seven) binding sites[30–32]. Therefore, lipid-conjugated molecules can bind to albumin and may have the properties to achieve particularization due to their hydrophobic interaction. Thus, the nano- or albumin-binding drug delivery system has great potential to provide benefits to the pharmacokinetics of LMWH; however, it is technically difficult to induce nanoparticle generation or albumin binding while maintaining most of the anticoagulant effect of heparin.

In order to overcome the problems of LMWH delivery, we designed a carrier-free heparin nanoparticle using LMWH and a hydrophobic alkylamine (octadecylamine), maintaining most of the anticoagulant (anti-Xa) activity of LMWH. Utilization of end-specific conjugation at the 2-N,6-O-disulfo-D-glucosamine (reducing end) of the LMWH structure led to simultaneous possession of an anticoagulant effect[33,34] so that possession of lipid molecules led to the formation of nanoparticles in aqueous solution[35,36]. This means that this synthesized low-molecular-weight heparin and octadecylamine conjugate (LMHO) forms a stable nanoparticle structure via self-assembly due to the amphiphilic properties with potential albumin binding ability (Fig. 1). We could confirm this by demonstrating the formation of these nanoparticles and the binding process with albumin using a computer simulation and transmission electron microscopy (TEM), which indicated the mechanism by which LMHO effectively circulates in the bloodstream for long periods without obvious side effects. The natural formation and disintegration of LMHO nanoparticles may lead to binding with nearby albumin, leading to a longer action time. As a result, the nano-sized LMHO molecules administered to mice have a very long half-life compared to conventional LMWH, with long-term therapeutic effects. In addition, it was shown that the nano-sized or albumin-bound LMHO molecules maintain their ability to react with protamine molecules for detoxification while still retaining their anticoagulant effect, which ensures a prolonged and effectively controlled therapeutic anticoagulation. This approach has shown great potential for improving the physicochemical properties of polysaccharides or heparins without inhibiting their therapeutic potency and with carrier-free nanoformulation and an auto-inducible albumin shuttling effect.

Results

Synthesis of LMWH–lipid conjugates through the site-specific reducing end of LMWH

Among the LMWHs, enoxaparin sodium, which is prepared by alkaline degradation[37–39], was utilized for chemical conjugation because it has the reactive 2-N,6-O-disulfo-D-glucosamine at the reducing end of the chain[6]. To achieve site-specific conjugation with alkylamine molecules, the end site of LMWH was reacted via a one-step protocol at 60 °C, with heating for 4 days (Fig. 2a). The reducing end site of LMWH selectively reacted by the primary amine of several hydrophobic alkylamines of different lengths, including hexylamine (C6), octylamine (C8), decylamine (C10), dodecylamine (C12), and octadecylamine (C18, ODA) in the presence of cyanoborohydride to reduce the imine to a secondary amine (Supplementary Fig. 1). As a result, several amphiphilic LMWH–lipid conjugates of various lipid lengths [LMWH–C6, LMWH–C8, LMWH–C10, LMWH–C12, and LMWH–C18 (LMHO)] were synthesized and purified (Fig. 2b). A typical fatty acid suitable for binding to the binding site of albumin consists of a carbon chain varying from 12 to 18 carbons in length[32], so five saturated medium-chain (C6, C8, C10, C12) and long-chain (C18) hydrophobic alkylamines were used for this purpose. The average reaction yield for these LMWH–lipid conjugates was approximately 61%.

The anti-Xa activity test with albumin binding

The anticoagulant activity of the synthesized LMWH–lipid conjugates was assessed by using the anti-Xa assay to confirm its therapeutic effect derived from the heparin part. As a result, the following anti-Xa activities of the various LMWH–lipid conjugates were determined: LMWH–C6 (102 ± 1%), LMWH–C8 (99 ± 7%), LMWH–C10 (83 ± 8%), LMWH–C12 (90 ± 4%), and LMWH–C18 (97 ± 3%) (Fig. 2c). The results indicate that the anti-Xa activities of LMWH–lipid conjugates are well preserved after synthesis and independent of the lipid lengths conjugated. We then evaluated the influence of lipid conjugation on the end site of LMWH by albumin at high (2%) or low (0.02%) concentrations to determine whether they bind to albumin and whether their anticoagulant effects are maintained after binding[40]. The binding potency ($ratio_{high/low}$) of LMWH–lipid molecules to albumin was calculated based on their change in anticoagulant effect due to molecular binding[41]. The results showed that the anti-Xa activity of all LMWH–lipid conjugates decreased at high concentrations after albumin incubation. Among them, LMHO (LMWH–C18) showed an 81.7 ± 1.2% in anti-Xa activity with 0.02% albumin and a 56.3 ± 12.4% activity with 2% albumin, resulting in a $ratio_{high/low}$ of 2.39. This indicates a higher binding potency compared to other conjugates including LMWH–C12 ($ratio_{high/low}$ = 2.26) and LMWH–C8 ($ratio_{high/low}$ = 1.57). Consequently, LMHO, which retained 97% of inherent anti-Xa activity and exhibited high albumin binding potency, was selected for further experiments among the LMWH–lipid conjugates.

https://doi.org/10.1038/s41467-024-50819-7

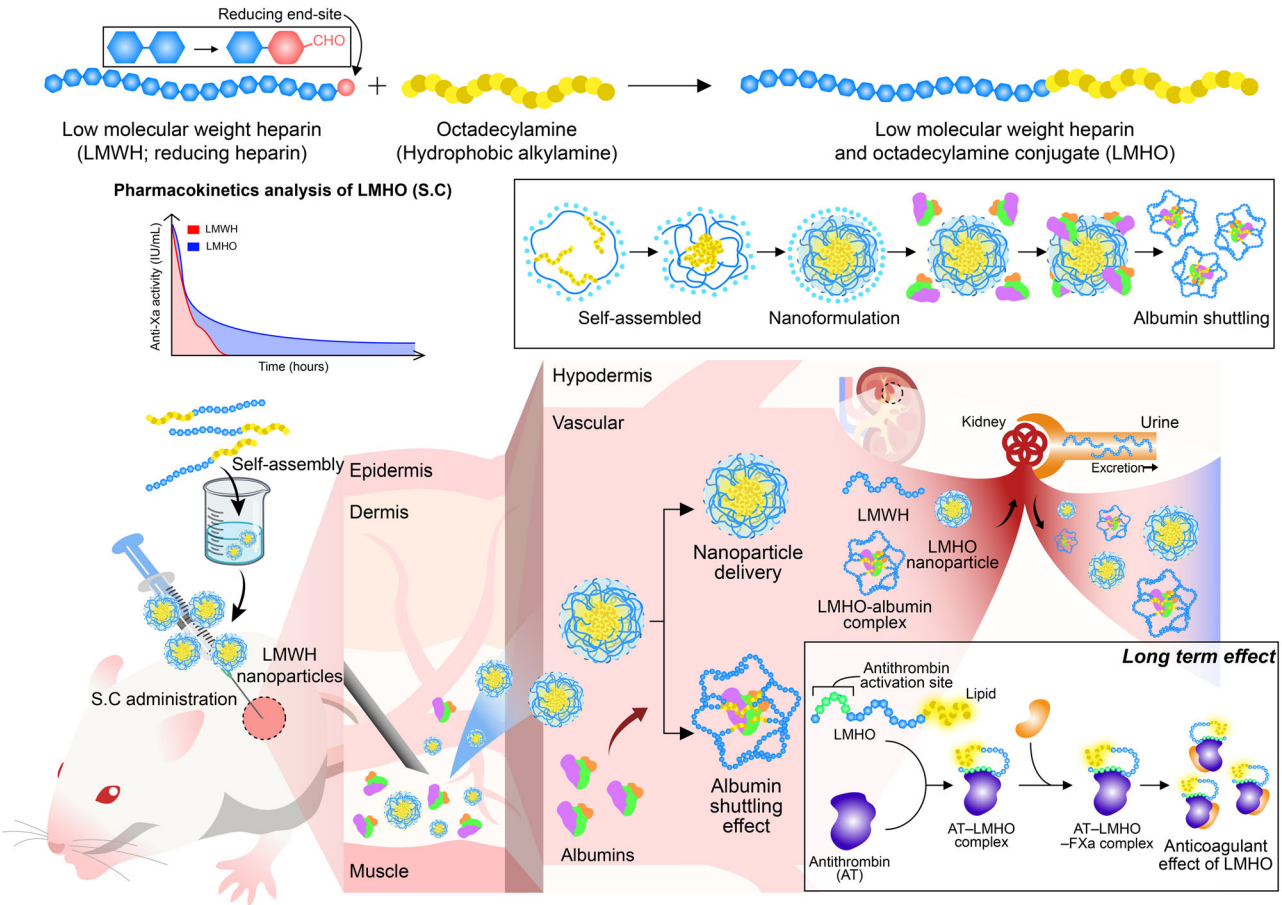

Fig. 1 | The schematic representation of self-assembly and albumin shuttling effect of LMHO. The heparin-based LMHO conjugates, entities that retain their anticoagulant activity through the specific reducing end (2-N,6-O-disulfo-D-glucosamine) present in LMWH (Enoxaparin), can self-assemble in aqueous conditions due to the hydrophobic nature of the conjugated octadecylamine. The carrier-free nanoformulation of LMHO also improves its capacity to bind to endogenous albumin in vivo as in albumin shuttling effect, enabling prolonged circulation in the bloodstream.

Characterization of LMWH–lipid conjugates

The synthesized and purified LMWH–lipid conjugates were confirmed using 1D-^{1}H NMR based on the lipid peak of the conjugates that were identified in the range of 0.7–1.3 ppm (Fig. 2e, Supplementary Figs. 2 and 3). In particular, in the case of LMHO, two-dimensional (2D) 800 MHz NMR with ^{1}H-^{13}C HSQC (heteronuclear single-quantum coherence) was used to evaluate the reaction with 2-N,6-O-disulfo-D-glucosamine of the end site of LMWH (Fig. 2f). The ^{1}H-^{13}C HSQC results of LMWH displayed the region of the trisulfated disaccharide, non-reducing end and reducing terminal residues. The ODA molecule reacted with a transiently generated aldehyde group at the terminal site (Supplementary Fig. 1), resulted in the absence of reducing terminal residues in the 5.4–5.5 ppm region (the lowest circle) following the synthesis of LMHO (Fig. 2f). Therefore, the HSQC spectra demonstrated the elimination of the reducing-end site region in LMWH, providing support for the specific end-site conjugation of LMHO. In addition, using diffusion-ordered NMR spectroscopy (DOSY-NMR), we compared the diffusion coefficient of LMHO to that of a mixture of LMWH and ODA to confirm molecular conjugation. LMHO demonstrated a diffusion rate of 1.73×10^{-10} m^2/s at 3.55 ppm and 1.94×10^{-10} m^2/s at 1.19 ppm (Supplementary Fig. 4). In contrast, the physical mixture displayed two distinct diffusion rates: 2.01×10^{-10} m^2/s for LMWH at 3.56 ppm and 1.02×10^{-9} m^2/s for ODA at 1.17 ppm; This indicates successful conjugation of ODA to the reducing end of LMWH. The absence of unconjugated ODA within the purified LMHO was further confirmed via RP-HPLC and the characteristic peak of unconjugated ODA, with a retention time of 32.4 min, was absent in the purified LMHO (Supplementary Fig. 5).

The successful conjugation of LMHO was further confirmed through nitrous acid degradation, which separated the synthesized compound into soluble degraded LMWH fragments and a precipitated ODA in distilled water (Fig. 2g). The precipitate was identified as ODA through 1D-^{1}H-NMR analysis, resulting from the decomposition of ODA that had been bound to LMHO (Fig. 2g). Based on the dry weight results that were not unaffected by the free amine of ODA, the conjugation ratio was calculated using the weight ratio of purified LMWH and ODA from the LMHO molecule (Fig. 2h). Mass analysis through acid digestion and precipitation showed that 20 mg of LMHO had successfully chemically decomposed into 1.14 mg of dried precipitate (ODA) and 18.85 mg of water-soluble materials (LMWH) after lyophilization. As a result, the ratio of LMWH to ODA in LMHO was determined to be 95.3 ± 0.1% (water-soluble; LMWH) to 4.7 ± 0.1% (water-insoluble; ODA), respectively. This means that the calculated binding mole ratio was 1:0.99, suggesting an almost 1:1 ratio. The theoretical highest binding ratio in the literature is 0.85[42,43], because enoxaparin has 15% of a 2-O-sulfo-4-enepyranosuronic acid group in the end site, but it appears to bind at a slightly higher ratio. It is generally known that the reaction of an aldehyde (at the end of heparin) with a primary amine (lipid) can form an imine derivative, also known as a Schiff base, but it is almost lost due to the presence of sodium cyanoborohydride ($NaCNBH_3$) (Supplementary Figs. 1 and 6).

The status of the reducing end of LMHO was further evaluated by verifying the existence of aldehyde groups and non-enzymatic

https://doi.org/10.1038/s41467-024-50819-7

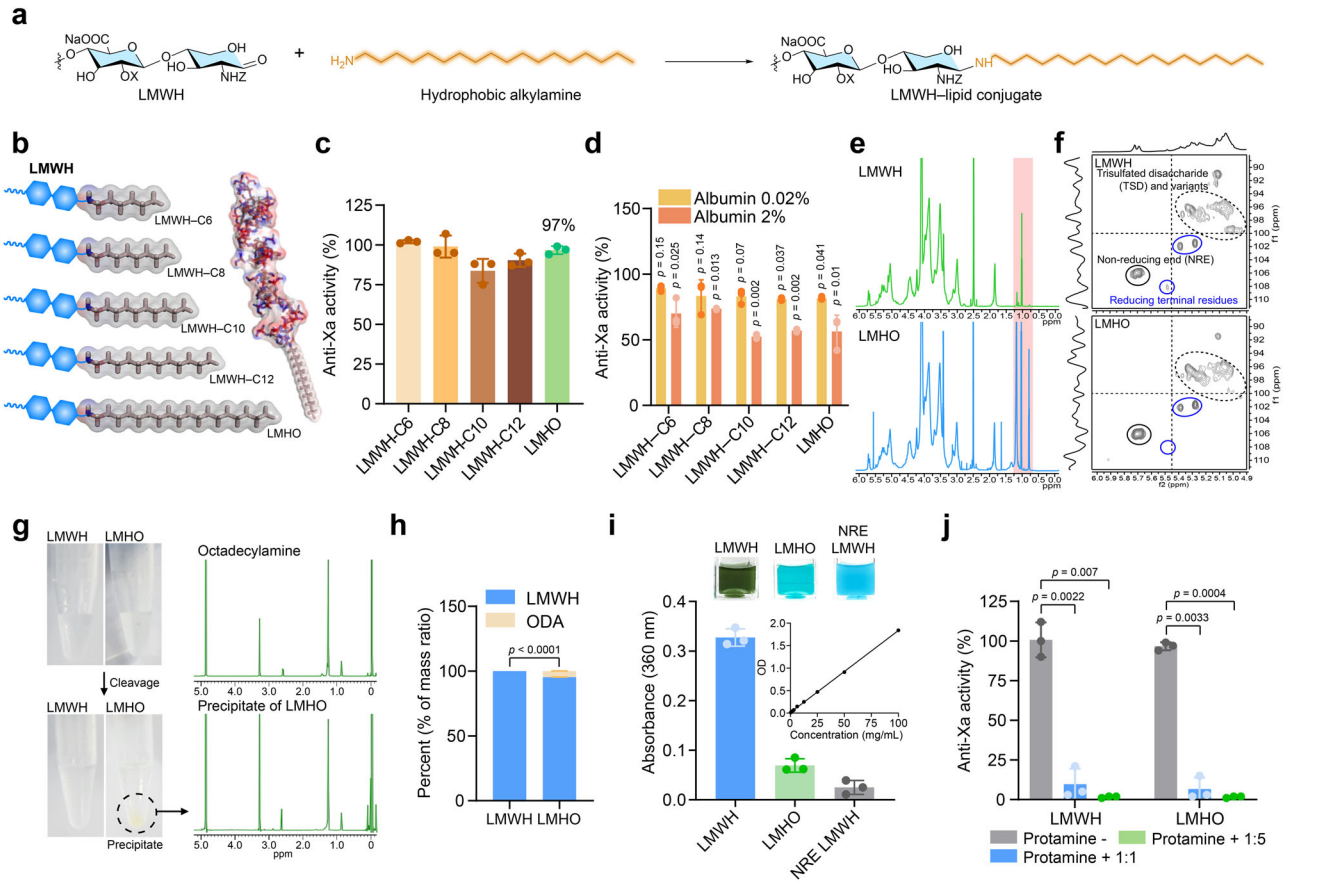

Fig. 2 | Synthesis and characterization of LMWH–lipid conjugates. Reducing sugar end-specific conjugation of LMWH with a hydrophobic alkylamine (**a**): Various synthesized LMWH–lipid conjugates including LMWH–C6, LMWH–C8, LMWH–C10, LMWH–C12, and LMWH–C18 (LMHO) (**b**). The anticoagulant (anti-Xa) activity of LMWH-lipid conjugates compared to LMWH (**c**) and under different albumin (HSA) concentrations of 0.02 or 2% ($n = 3$ independent samples, one-way ANOVA with Dunnett' test for p value) (**d**). 1D proton NMR results with octadecylamine peak (pink shading) (**e**) and 2D ^{1}H-^{13}C HSQC NMR results (**f**) of LMWH with reducing end and LMHO. **g** Nitrous acid depolymerization for heparin degradation and ^{1}H-NMR data of water-insoluble ODA of LMWH and LMHO. **h** Mass ratio analysis after nitrous acid depolymerization of LMWH and LMHO ($n = 3$ independent samples, unpaired t-test for p value). **i** Non-enzymatic glycosylation of LMHO and NRE–LMWH (non-reducing end LMWH; nadroparin) was compared to LMWH (reducing end LMWH; enoxaparin), which has a terminal reducing sugar moiety, resulting in solution color change upon reaction with Benedict's reagent. ($n = 3$ independent samples). **j** In vitro protamine neutralizing test in buffer at 1:1 or 1:5 ratios. ($n = 3$ independent samples, one-way ANOVA with Dunnett' test for p value). Data are presented as mean values ± SD. Source data are provided as a Source Data file.

glycosylation utilizing Benedict's reagent with LMWH[44]. LMWH or LMHO was dissolved in Benedict's reagent at a concentration of 40 mg/mL. The LMWH solution of enoxaparin sodium, which has a reducing sugar in the end, displayed a remarkable color change, whereas the color of the LMHO solution remained constant (Supplementary Fig. 7). Another NRE-LMWH named nadroparin (Avg M.W. 4.3 kDa) was examined using the same method for comparison. NRE-LMWH molecules have a characteristic inactivated NRE (2,5-anhydro-D-mannose) group at the reducing terminus because they are chemically depolymerized from unfractionated heparin (UFH) using periodate oxidation. Consequently, the color of the NRE-LMWH solution also remained unchanged. After 6 h of non-enzymatic glycosylation, the UV/Vis absorbance measured after reacting with Benedict's reagent showed that LMWH with a reducing end exhibited an absorbance of 0.327 ± 0.017. In contrast, the absorbance for LMHO decreased to 0.069 ± 0.014, which is comparable to the 0.025 ± 0.014 observed for non-reducing end LMWH (NRE-LMWH), implying that the end site of LMHO was inactivated due to ODA binding (Fig. 2i and Supplementary Fig. 7).

In vitro neutralization by protamine

The neutralization capacity of LMHO by its antidote, protamine, was assessed by evaluating their anticoagulant activity in the presence of protamine molecules at two concentration ratios (1:1 and 1:5), within PBS buffer or rat plasma. The protamine treatment at a 1:1 ratio resulted in reduced anticoagulant activities of 9.7 ± 9.9% for LMWH and 6.7 ± 7.2% for LMHO (Fig. 2j). At the higher protamine concentration of 1:5, both molecules demonstrated very low anticoagulant activity, with LMWH at 1.7 ± 0.6% and LMHO at 1.5 ± 0.5%, indicating effective protamine-based neutralization potential. Additionally, the neutralization capacity of both molecules in plasma was slightly diminished in comparison to the buffer group, exhibiting values of 65.3 ± 3.5% for LMWH and 45.7 ± 6.0% for LMHO (Supplementary Fig. 8). Consequently, LMHO demonstrated adequate reversibility when exposed to protamine, similar to that observed with LMWH, highlighting its controllable potential for therapy.

Molecular dynamic simulation for self-assembled LMHO

We speculated that the binding of hydrophilic LMWH to hydrophobic alkylamine groups imparts amphiphilic properties, which could lead to the formation of self-assembling nanoparticles. To demonstrate the nanoformulation of LMHO in silico, molecular dynamics (MD) simulation was conducted from 0 to 500 ps. by using BIOVIA Discovery Studio software. In the CHARMM (Chemistry at Harvard Macromolecular Mechanics) force field, LMHO molecules formed self-assembling nanoparticles stably over time by positioning

hydrophobic groups in the center (Fig. 3a). The calculated van der Waals energy changed from −2119.72 to −2676.28 kcal/mol when comparing 2 and 500 ps with transition to a more stable state (Fig. 3b), and the number of their hydrophobic interactions was increased to 100 ps possibly due to carbon chain (Supplementary Fig. 9). The number of H-bonds of the simulated LMHO nanoformulation increased from 53 to 220 (Fig. 3b), which is a 4.2-fold increase, indicating molecular interactions between heparin molecules had also become more complex. Furthermore, when the simulation time was extended to 10 ns, the stability of the self-assembled nanoparticles was maintained up to 10 ns significant change throughout the period (Supplementary Fig. 10). This indicates that the formation of self-assembled LMHO nanoparticles is rapidly completed within 500 ps to 2 ns.

Characterization of self-assembled LMHO nanoparticles

The self-assembled nanoparticle of LMHO was directly characterized using dynamic light scattering (DLS). The particle size distribution of LMHO was measured to be 127.1 ± 0.7 nm (Fig. 3c), with a zeta potential of −54.29 ± 4.3 mV (Fig. 3d). LMHO molecules formed stable self-assembled nanoparticles with a polydispersity index (PDI) of 0.2186. However, LMWH–C8, the conjugate of LMWH and a shorter alkylamine, exhibited relatively unstable particle formation, with a Z-average size of 561.7 nm and a high PDI value of 0.7447 (Supplementary Fig. 11). Particle observations using TEM and scanning electron microscope (SEM) imaging showed the spherical shape of self-assembled LMHO nanoparticles (Fig. 3e, f), with a size of around 200 nm, matching the DLS data in Fig. 3c. For a more detailed nanoparticle analysis, we incorporated the fluorescent dye cyanine 5.5 (Cy5.5) into the carboxyl group of LMHO molecules. Then, the formation of these self-assembled nanoparticles was assessed by measuring the fluorescence intensity of Cy5.5-conjugated LMHO. At first, the fluorescence intensity was weak, possibly due to self-quenching, and when exposed to DMSO solutions ranging from 0% to 75%, the fluorescence intensity of LMHO increased approximately 23-fold, from 294.3 ± 25.1 (DMSO 0%) to 6880.4 ± 207.8 (DMSO 75%) (Fig. 3g). The results show that DMSO hinders the hydrophobic interaction of LMHO nanoparticles, leading to enhanced exposure of the Cy5.5 fluorescent molecules. Correspondingly, nanoparticle formation was also confirmed by conducting a comparative analysis of ^{1}H-NMR, which revealed a change in ODA intensity (Fig. 3h). It was observed that hydrophobic ODA groups, which were not visible in 100% water in ^{1}H-NMR, were significantly detected as the organic solvent (DMSO) content increased (0% to 75%).

The particle stability of LMHO was compared by measuring the particle size at different time points (1, 3, 6, 12, 24, 48 and 72 h) for a more detailed nanoparticle characterization. The LMHO particles maintained a particle size below 200 nm for up to 72 h, showing high particle stability in serum, Dulbecco's Phosphate-Buffered Saline (DPBS), or normal saline (Fig. 3i). They displayed similar behavior for up to 24 h in other solutions such as DMEM or distilled water (DW) (Supplementary Fig. 12). Additionally, other LMWH–lipid conjugates were also to analyze whether this stability may be contributed by the long carbon chain. The measurements showed that LMWH–lipid conjugates with varying lipid lengths (LMWH–C6, –C8, –C10, and –C12) exhibited different degrees of particle stability in serum, showing no specific pattern for carbon length (Supplementary Fig. 13). LMWH–C6 and LMWH–C12 remained stable, whereas LMWH–C8 and LMWH–C10 underwent significant size increases and became unstable after only 3 h.

In vitro cytotoxicity assay

A cell viability assay was conducted on three cell lines—human-derived lung (MRC-5), canine kidney (MDCK), and adult human dermal fibroblasts (HDFa)—to assess the potential cytotoxicity of synthesized amphiphilic LMHO molecule. Treatment with the highest concentration of 100 μg/mL of LMWH and LMHO resulted in the following cell viability percentages: HDFa cell line 96.0 ± 8.2% (LMWH), 93.6 ± 6.4% (LMHO) (Fig. 3j); MRC-5 cell line 97.4 ± 3.5% (LMWH), 93.2 ± 5.7% (LMHO); MDCK cell line 97.2 ± 5.3% (LMWH), 96.6 ± 6.8% (LMHO). These results demonstrate the low cytotoxicity of LMHO. (Supplementary Fig. 14).

Albumin binding of LMHO nanoparticles

The interaction between LMHO and albumin was confirmed by comparing the particle size distribution of albumin at different ratios of LMHO (1:0 (LMHO/albumin), 1:1, 1:10, and 1:100) using DLS (dynamic light scattering). When albumin with a concentration of 0.1 mg/mL was dissolved in DW, its particle size distribution was approximately 6.4 ± 1.1 nm (Supplementary Fig. 15). However, when LMHO solution was added to this solution at the same ratio, 1:1 (LMHO/albumin), the z-average size was increased to 9.7 ± 1.5 nm (Fig. 4a) with nanoparticles (Avg. 100 nm). This could be due to the molecular movement of LMHO by binding to albumin through hydrophobic interactions, causing an increase in size. As the ratio of albumin increases, the ratio of 100 nm LMHO particles decreases, suggesting increased binding of LMHO with an increased availability of albumin (Fig. 4a).

To compare the affinity of binding to albumin, LMWH and LMHO molecules labeled with rhodamine B isothiocyanate (RITC) were evaluated using an albumin-coated agarose spin column. They were incubated in the column coated with albumin for an hour which was then washed four times with DPBS. As a result, the column treated with LMHO–RITC showed a higher intensity than the one treated with LMWH–RITC, suggesting a greater affinity of LMHO toward albumin compared to LMWH (Fig. 4b). The fluorescence intensity of LMWH–RITC was 411.3 ± 10.6 (Arb. u.), while that of LMHO–RITC was twice as high, measuring 871.7 ± 46.3 (Arb. u.) (Fig. 4b).

The albumin-binding specificity of LMHO was further assessed by measuring the intensity of Cy5.5 bound to albumin on native PAGE after co-dissolving LMWH–Cy5.5 or LMHO–Cy5.5 with HSA. LMHO–Cy5.5 was bound to albumin and loaded slowly, displaying a high intensity at the top of the gel. In contrast, LMWH–Cy5.5, which did not bind as strongly to albumin, was observed at the bottom of the gel as shown in Fig. 4c. This difference illustrates the higher albumin binding affinity of LMHO compared to LMWH. LMHO–Cy5.5 exhibited a 3.7-fold increase in bound albumin intensity compared to LMWH–Cy5.5 (Fig. 4d).

To analyze the interaction between albumin and LMHO nanoparticles at the molecular level, MD simulation was conducted using albumin and LMHO molecules. At first, a docking simulation between LMHO fragments and albumin molecules was performed based on the albumin protein (PDB: 1E7H) considering approximately seven binding sites[32] of lipid in albumin, and the LMHO fragment showed a slightly high binding affinity to the albumin structure (Supplementary Fig. 16). Subsequently, MD simulations were conducted to investigate the interactions between LMHO nanoparticle molecules and an albumin protein, elucidating the molecular mechanisms behind the formation, migration, and binding of LMHO molecules to albumin (Fig. 4e) by using BIOVIA Discovery Studio software. As a result, the interaction between the compound and albumin continued due to the presence of the hydrophobic alkyl group, which eventually results in binding to the fatty acid binding site of albumin in a distance-dependent dielectric implicit solvent model.

The interaction between LMHO and albumin was further confirmed through TEM and bio-layer interferometry (BLI). The TEM images show LMHO nanoparticles with a mean size of 214.3 ± 63.1 nm (Fig. 3e), while free albumin was not clearly observed in TEM analysis (Supplementary Fig. 17). Interestingly, after mixing LMHO nanoparticles with albumin, more complex shapes of nanoparticles and albumin molecules were observed. A large number of nanoparticles that were bound to albumin or degraded were observed, which could

https://doi.org/10.1038/s41467-024-50819-7

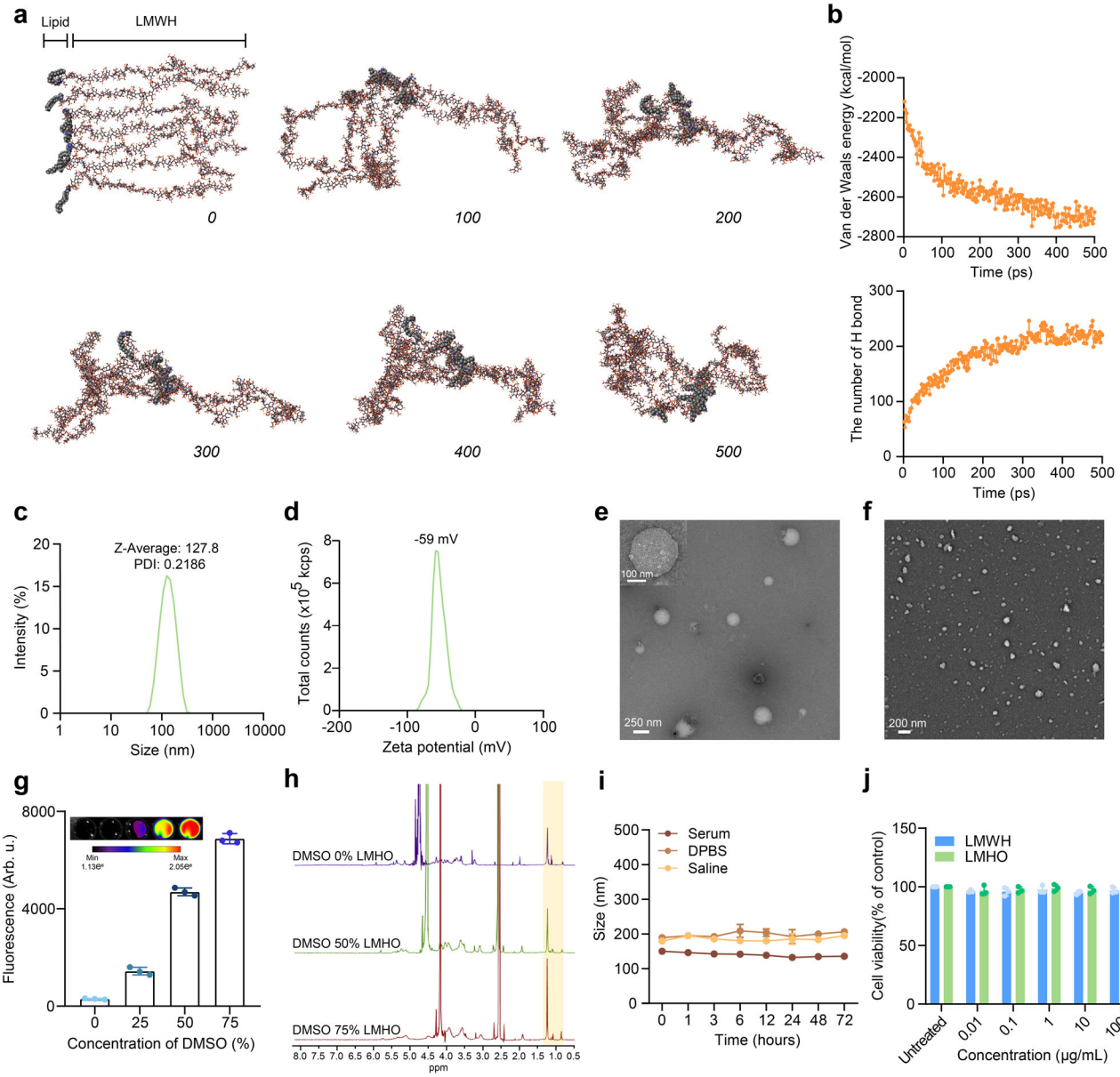

Fig. 3 | Nanoformulation and molecular dynamics analysis. a MD simulation of self-assembled LMHO with a core hydrophobic octadecylamine residue in the implicit (distance-dependent dielectric) solvent model between 0 and 500 ps. **b** Total van der Waals energy and the number of H bonds calculated in MD simulations of LMHO. Particle size distribution (**c**) zeta potential (**d**) **e**, **f** representative transmission electron microscopy (TEM) image and field emission scanning electron microscopy (FE-SEM) image ($n = 3$ independent experiments) of LMHO nanoparticles. Fluorescence changes (arbitrary units, Arb. u.), ($n = 3$ independent experiments) (**g**) and ^{1}H-NMR results with octadecylamine peak (yellow shading) (**h**) according to the disintegration of LMHO nanoparticles by organic solvent (DMSO). **i** Stability of LMHO nanoparticles over time (up to 72 h) under various solvent conditions ($n = 3$ independent samples). **j** The cytotoxic effect on HDFa normal cells was evaluated within the concentration range of 0.01–100 μg/mL for 24 h ($n = 6$ samples for 3 independent experiments). Data are presented as the mean values ± SD. Source data are provided as a Source Data file.

explain the disassembly of the self-assembled nanoparticles and their migration to albumin molecules (Fig. 4f). Furthermore, HSA was immobilized on an amine-reactive sensor to analyze the nanoparticles' interactions with albumin by bio-layer interferometry (BLI) analysis. Since LMWH does not react with albumin, the K_D (M) value of LMWH was not determined in the BLI assay with HSA molecules. However, LMHO showed a remarkable K_D value of 7.53×10^{-9} (Fig. 4g), indicating a high affinity for albumin molecules.

Pharmacokinetic study

The pharmacokinetics of LMHO and LMWH in the body were evaluated by comparing their anti-FXa profiles. When LMWH or LMHO were administered at a dose of 5 mg/kg via intravenous (I.V.) or subcutaneous (S.C.) routes, there was no difference in the anti-FXa activity profile during the first hour after their injection. However, while LMWH was almost eliminated 8 h after administration, LMHO remained at around 0.23 ± 0.07 IU/mL (I.V.) and 0.25 ± 0.07 IU/mL (S.C.) even up to 72 h (Fig. 5a and Supplementary Table 1). The half-life ($t_{1/2}$) of LMHO was 65.3 h, which is 45.4 times longer than the 1.44-h half-life of LMWH. Furthermore, when calculating the area under the curve (AUC) using non-compartment analysis, LMWH and LMHO showed values of 29.13 ± 2.98 h·μg·mL^{-1} and 243.42 ± 26.70 h·μg·mL^{-1}, respectively, indicating that LMHO had an approximately 8.4 times higher AUC (Fig. 5b). Additionally, changes in the pharmacokinetic properties of LMWH–lipid nanoparticles were assessed in relation to the formation of self-assembled nanoparticles. When LMHO molecules

https://doi.org/10.1038/s41467-024-50819-7

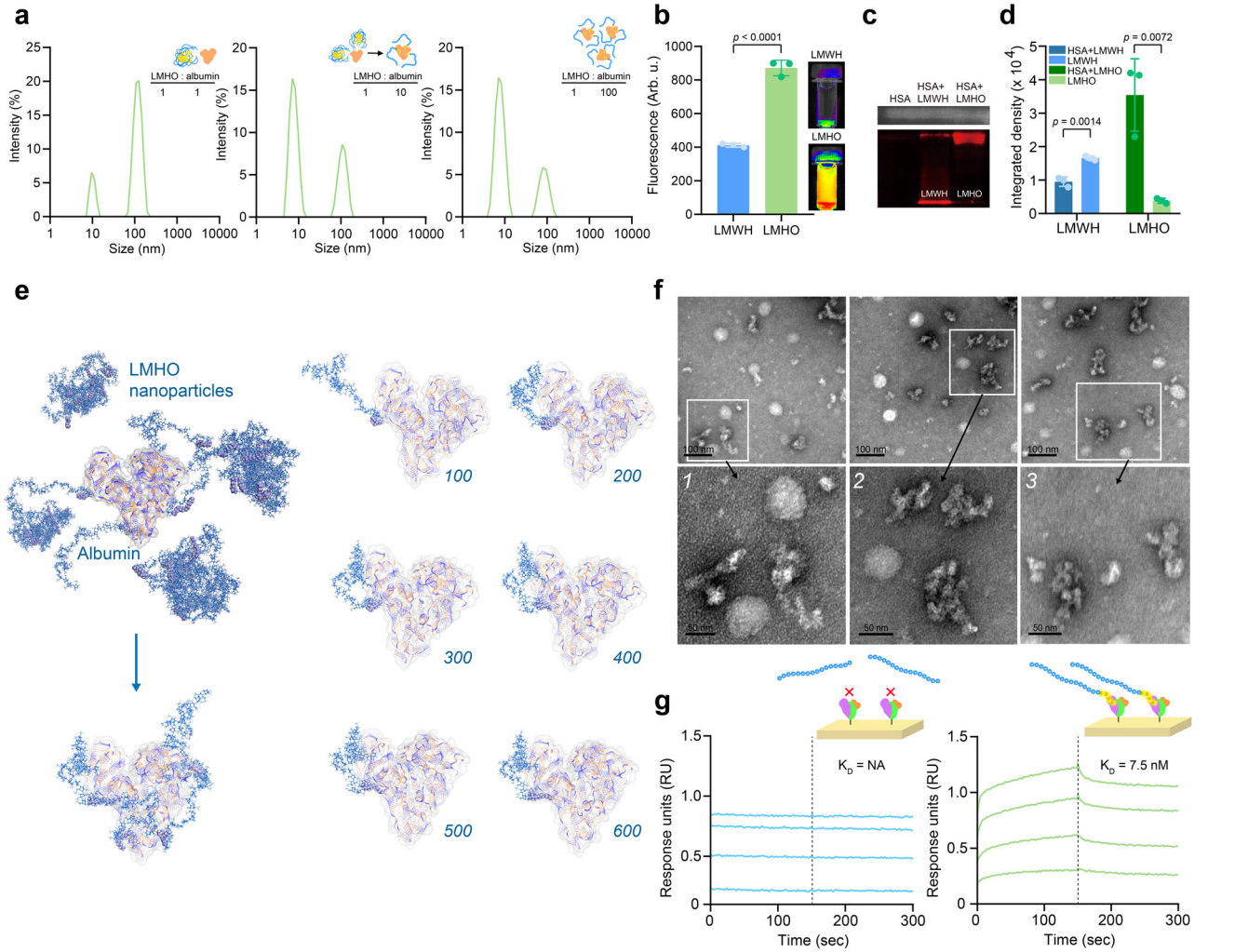

Fig. 4 | Interaction analysis between LMHO and albumin. a Size distribution of LMHO interacting with albumin (1:1, 1:10, and 1:100). In vitro albumin binding assay using albumin-coated agarose gel columns ($n = 3$ independent samples, unpaired t-test for p value) (**b**) and native PAGE analysis (**c**) using fluorescence-labeled LMWH and LMHO molecules (arbitrary units, Arb. u). **d** Quantitation of fluorescence-labeled LMWH and LMHO bound to albumin protein ($n = 3$ independent samples, unpaired t-test for p value). **e** MD simulation to investigate the interaction between LMHO and albumin for 600 ps. Representative transmission electron microscopy (TEM) images ($n = 3$ independent experiments) (**f**) and bio-layer interferometry (BLI) results (**g**) between LMHO and albumin. Data are presented as mean values ± SD. Source data are provided as a Source Data file.

were bound with rat albumin prior to self-assembly (albumin-pretreated LMHO), their plasma half-life decreased to 13.17 h following subcutaneous (S.C.) administration (Supplementary Fig. 18). Furthermore, unstable LMWH–lipid nanoparticles (LMWH–C8) showed a reduced half-life (27.34 h) in Sprague-Dawley rats after S.C. administration. This suggests that the stable self-assembled nanoparticles of LMHO contribute to an increased plasma half-life in vivo with their albumin shuttling effect.

Dye-conjugated LMWH or LMHO was used to directly analyze their plasma concentration in the body after injection by analyzing the time course of RITC intensity (3, 6, and 12 h). LMWH–RITC was rapidly eliminated within 6 h (11.1 ± 11.2 Arb. u.), while LMHO–RITC maintained a high intensity even up to 12 h (79.7 ± 25.3 Arb. u.) (Fig. 5c). This long-term action could be a complex effect of nanoparticle formation and albumin binding, so we conducted an albumin binding analysis using plasma. The albumin binding specificity of LMHO was evaluated by administering LMHO–Cy5.5, followed by measuring the intensity of Cy5.5 bound to albumin in the plasma after 1 h. It was confirmed that LMHO was largely distributed at the position of albumin using blot analysis (Fig. 5d). LMHO–Cy5.5 showed an increase of 5.9-fold intensity in bound albumin compared to LMWH–Cy5.5 (Fig. 5e).

In vivo tail bleeding test in mice

The in vivo anticoagulant effect of LMHO and LMWH was compared through a tail bleeding experiment. They were dissolved in 100 μL of saline at a concentration of 5 mg/mL before being subcutaneously administered to the mice, and then an hour later, the prolongation of the clotting time due to heparin was compared. The primary coagulation time of the control group (saline) was 327 ± 183 s, whereas those of the LMWH and LMHO groups were prolonged with 3145 ± 433 s (LMWH) and 4450 ± 2074 s (LMHO), indicating that the blood coagulation time of was more delayed by treatment with LMHO than with LMWH (Fig. 5f).

Long-term anti-FXa activity following repeated dosing

The sustained anti-FXa activity of LMHO with a long half-life and repeated dosing was compared for up to 144 h. Additional administration followed at the 60 and 132 h, in accordance with the half-life of LMHO, which was determined to be 65.3 h. The findings indicated that a rapid decline in the anti-FXa activities of LMWH was observed within 6 or 12 h of treatment, resulting in levels lower than 0.2 IU/mL for an extended duration of 144 h. In contrast, it was observed that LMHO exhibited a consistent anti-FXa activity level of 0.2–0.4 IU/mL, which is

https://doi.org/10.1038/s41467-024-50819-7

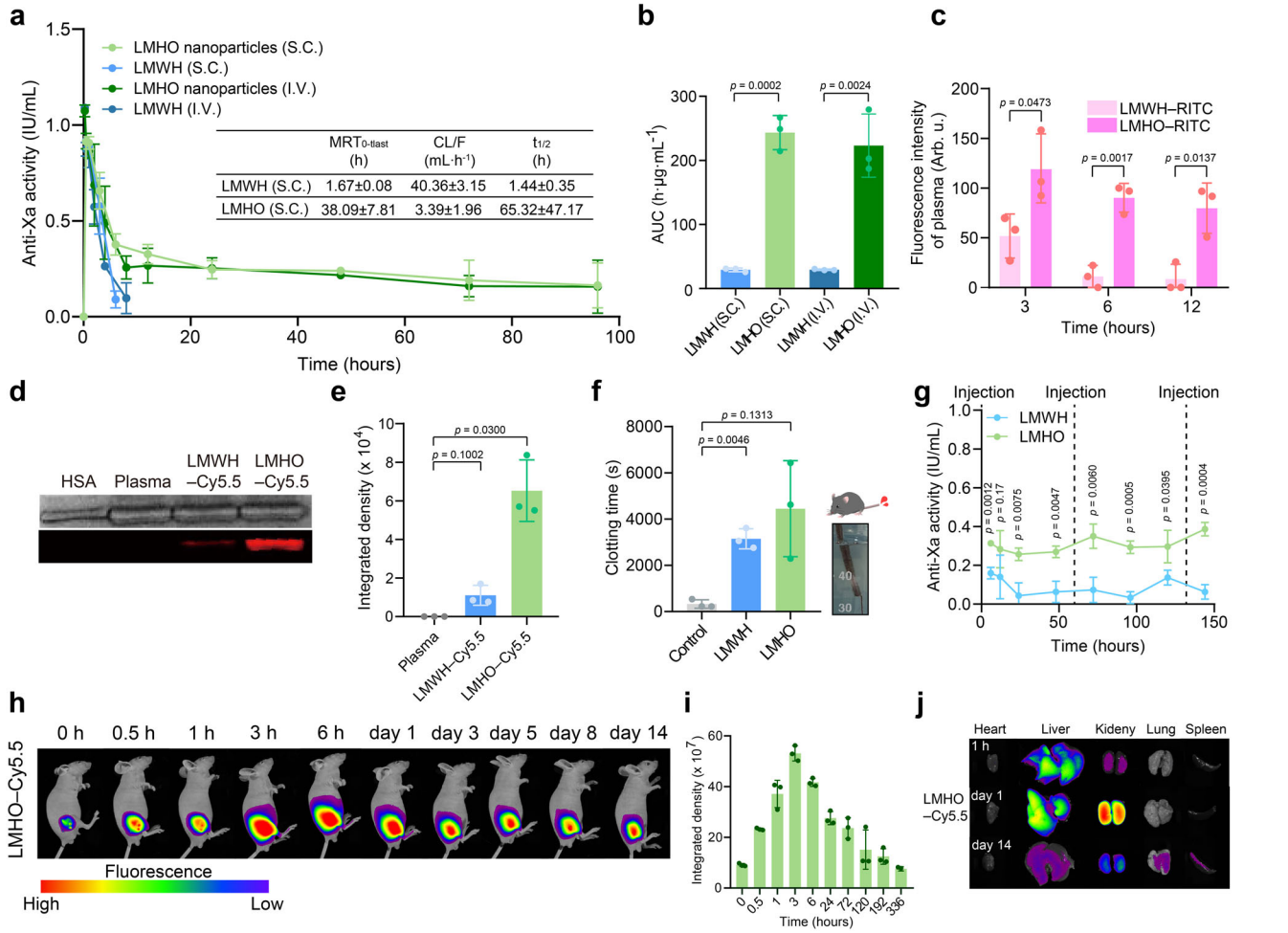

Fig. 5 | In vivo pharmacokinetic analysis and biodistribution of LMHO. Anti-Xa activities over time (**a**) and their area under the curve (AUC) (**b**) following single administration (S.C. or I.V.) of LMWH (5 mg/kg) and LMHO nanoparticles (5 mg/kg) to Sprague-Dawley rats ($n = 3$ rats, unpaired t-test for p value). Pharmacokinetic parameters (MRT, mean residence time; CL, clearance; F, dose; $t_{1/2}$, half-life) are estimated using non-compartment analysis. **c** Plasma fluorescence intensity (arbitrary units, Arb. u.) 3, 6, and 12 h after administration of LMWH–RITC (10 mg/kg) or LMHO–RITC (10 mg/kg) injection ($n = 3$ independent samples, unpaired t-test for p value). In vivo albumin-binding assay using a native PAGE assay an hour after administration of Cy5.5-labeled LMWH and LMHO (**d**), and its quantitative analysis ($n = 3$ independent samples, one-way ANOVA with Dunnett' test for p value) (**e**). **f** Tail clotting time comparison after cutting the tail of groups treated with administration of saline (control), LMWH, or LMHO ($n = 3$ mice, one-way ANOVA with Dunnett' test for p value). **g** The sustained anticoagulant effect of LMHO and LMWH for up to 144 h ($n = 3$ rats, unpaired t-test for p value) after repeated dosing. In vivo biodistribution of Cy5.5-labeled LMHO in BALB/c nude mice (**h**) and its integrated density of each point ($n = 3$ mice) (**i**). **j** Fluorescence analysis of the heart, liver, kidney, lung, and spleen at 1 h and day 1 and 14 after the administration of Cy5.5-labeled LMHO ($n = 3$ independent samples). Data are presented as mean values ± SD. Source data are provided as a Source Data file.

in line with its prolonged half-life (Fig. 5g). This means that LMHO has the potential to provide prolonged safe application, a challenge that has thus far been unable to be accomplished with heparin compounds.

In vivo biodistribution of LMHO

The LMHO–Cy5.5 (5 mg/kg) was subcutaneously administered to investigate the detailed biodistribution of LMHO in the body, and its fluorescence intensity was measured using a fluorescence analyzer (FOBI, CELLGENTEK, Republic of Korea) over 14 days. Most of the subcutaneously injected LMHO–Cy5.5 molecules were observed around the same injection site, unlike LMWH–Cy5.5 (Fig. 5h and Supplementary Fig. 19a), and the highest fluorescence intensity was observed at 3 h after administration (Fig. 5i and Supplementary Fig. 19b), indicating the dissolution and dispersion of self-assembled heparin nanoparticles, some of which might have bound to albumin in a monomolecular state at the nanoscale. Compared to LMWH–Cy5.5 at 1 day after administration, the kidneys of LMHO–Cy5.5 showed higher fluorescence intensity, indicating that the excretion and elimination primarily occur in the kidneys (Fig. 5j and Supplementary Fig. 19c). However, LMWH–Cy5.5 had a higher intensity in the liver tissue on day 1 than LMHO–Cy5.5 (Supplementary Fig. 20). Given that the metabolization and excretion of low-molecular-weight heparin proceeds in the liver, these results suggest that the metabolization of LMHO might be altered.

In vivo protamine reversibility test

Protamine sulfate, a peptide with a highly positive charge, is commonly used to neutralize the anticoagulant effect of LMWH by binding to it, which is one of the advantages of heparin as an anticoagulant[45]. The in vivo reversibility of the anti-FXa activity by protamine was investigated for LMHO to determine whether it can react with protamine in the blood to maintain this action and act as an antidote. After 3 h of subcutaneously administering LMHO in mice, protamine sulfate (25 mg/kg) was intravenously injected to neutralize the effects of heparin. As a result, both LMWH and LMHO showed decreased anti-FXa activity levels of 0.09 ± 0.06 IU/mL (LMWH) and 0.003 ± 0.006 IU/mL (LMHO) by protamine at 3 h (Fig. 6a). Without the protamine injection, the levels were maintained as 0.41 ± 0.01 IU/mL (LMWH) and 0.56 ± 0.03 IU/mL (LMHO).

https://doi.org/10.1038/s41467-024-50819-7

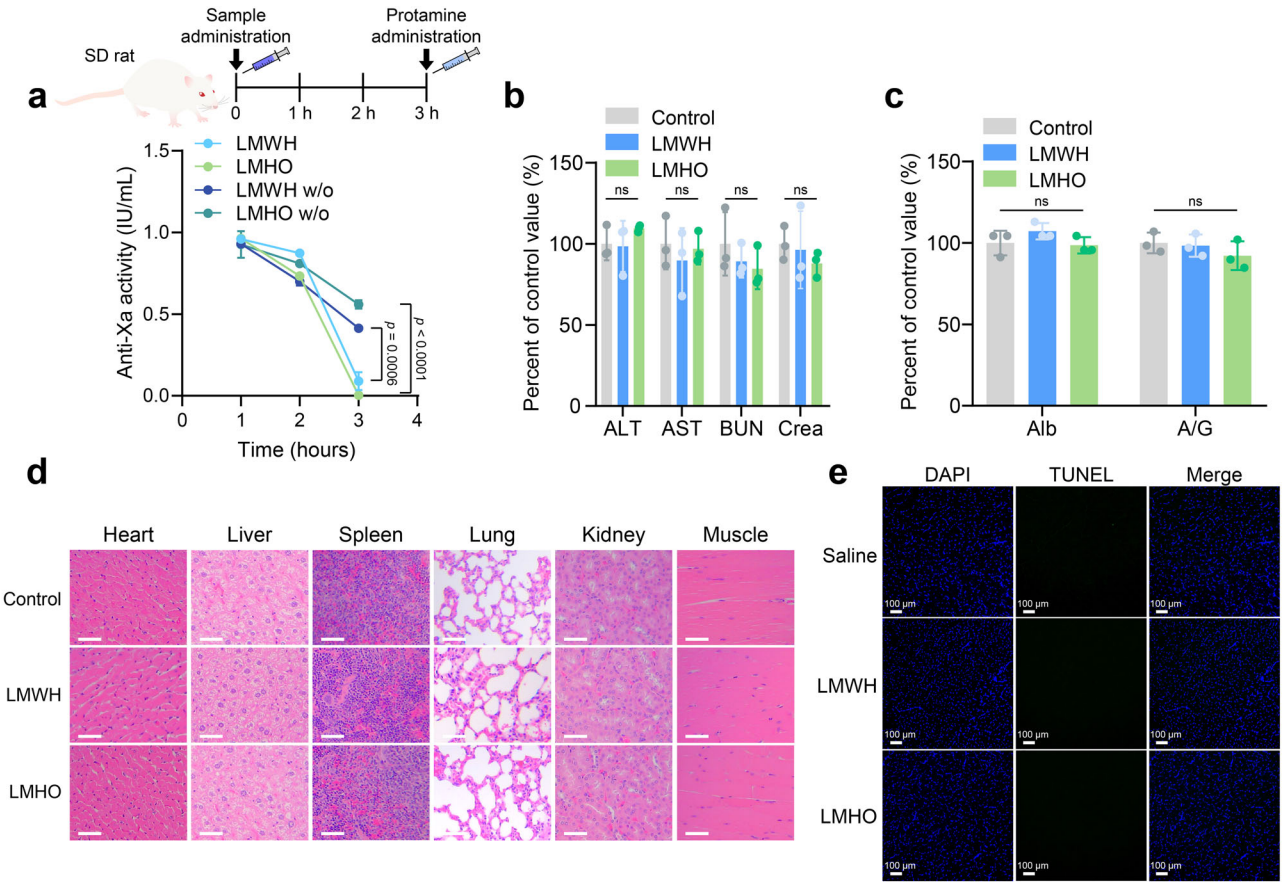

Fig. 6 | In vivo systemic and histopathological toxicity of LMHO. a In vivo FXa activity of LMHO that was neutralized by protamine compared to LMWH ($n = 3$ rats, unpaired t-test for p value). Liver function parameters including alanine transaminase (ALT), aspartate transaminase (AST), albumin (Alb) (**b**), and albumin/globulin (A/G) (**c**) in the serum. $p > 0.05$ (ns) ($n = 3$ independent samples, unpaired t-test for p value). Representative H&E staining (scale bars, 50 μm) of the heart, liver, spleen, lung, kidney, and muscle on the injection site (**d**) and TUNEL staining (scale bars, 100 μm) on the injection site (**e**) in Sprague-Dawley rats ($n = 3$ independent samples). Data are presented as mean values ± SD. Source data are provided as a Source Data file.

Systemic and histological toxicity of LMHO

After the administration of LMHO (5 mg/kg, S.C.), the systemic toxicity related to the liver and kidneys, as well as histological toxicity in various tissues, were evaluated and compared with the LMWH and control groups. In both the LMWH- and LMHO-treated groups, there were no significant differences compared to the control group in terms of alanine aminotransferase (ALT), aminotransferase (AST), urea nitrogen (BUN), and creatinine levels (Fig. 6b). Using albumin in the body after injection, it is possible to show the changed ratio of albumin in the blood or kidney toxicity, but no toxicity was observed (Fig. 6c). Similarly, the levels of Na, K, and Cl were also not significantly different from the control group (Supplementary Fig. 21). In addition, histological examination using H&E (hematoxylin and eosin) staining of the heart, liver, spleen, lung, and kidney did not show any difference to the control, demonstrating that there was no significant systemic or local toxicity observed in LMHO (Fig. 6d). TUNEL (terminal deoxynucleotidyl transferase dUTP nick end labeling) staining of the muscle at the injection site also did not reveal any difference to the control, indicating that heparin can be delivered without significant toxicity (Fig. 6e and Supplementary Fig. 22).

Discussion

Continuous and effective delivery of functional polysaccharides for therapy has presented technical limitations due to their high molecular weight and strong charge. It was difficult to develop a general strategy that was controlled by trapping in hydrophobic nanoparticles (e.g., PLGA NP); no similar heparin derivatives or conjugates have been researched and developed to date. Numerous studies have utilized polysaccharide-based nanoparticles for other purposes, such as anticancer drug delivery or theragnostics, maintaining some functions of polysaccharides[46,47]. In this study, a hydrophobic alkyl motif was introduced into LMWH molecules to generate self-assembled LMWH nanoparticles. This approach was based on reports that lipids of appropriate lengths can form micelles in water[48–50]. Initially, we hypothesized that LMWH with a hydrophobic alkyl motif could not only intrinsically form nanoparticles but also induce an albumin binding effect. However, direct lipid or drug conjugation (e.g., doxorubicin or bile acids) to the LMWH molecule is generally associated with loss of the anticoagulant effect of heparin[16,51]. Therefore, we prepared a self-assembled octadecylamine-based LMWH conjugate (LMHO) capable of binding to albumin that fully maintained its functions by utilizing the reducing sugar of LMWH. For reducing end binding, enoxaparin was specifically used; most of the anticoagulant effect was maintained (97%) after 4 days of the chemical reaction (Fig. 2a, c).

Although the relationship between lipid groups, nanoparticles, and albumin has been studied many times, few experiments have validated both the self-assembling nanoparticles themselves and their binding to albumin[52–54]. Albumin can shuttle lipids in the bloodstream by binding to them, so the complex that can be formed between albumin and fatty acids is called an albumin–fatty acid complex[31]. Albumin helps solubilize and transport these lipids, ensuring they can reach their intended destinations within the body's tissues[22]. Since polysaccharide molecules are highly hydrophilic and flexible, it was

not clear whether albumin can bind or utilize the lipid part of the LMWH–lipid conjugate. However, our results showed that the hydrophobic octadecyl group appropriately contributed to the formation of self-assembled nanoparticles of LMHO with binding to albumin (Fig. 4e, f). However, as the molecular size of LMHO approaches albumin, it may be difficult to bind, but binding was nevertheless shown in the simulation results and verified through TEM imaging.

In terms of preventive anticoagulant therapy, long-term continuous and effective action is important because the molecular action of heparin lies in the prevention rather than the treatment of several diseases. Moreover, anticoagulants should be adjustable to maintain their action for a desired period of time, because they can present a risk of bleeding for the patient. LMHO can form self-assembled nanoparticles and bind to albumin to exhibit long-term anticoagulant effects, while at the same time possessing the ability to reduce LMWH activity by the treatment of protamine (Figs. 4c and 6a)[45]. As a result, the anticoagulant effect could be successfully controlled due to the administration of protamine, which means that the effect can be controlled clinically in the future. However, due to the continuous release of LMHO from nanoparticles, perfect control may not be possible through a single administration of protamine but resolved through numerous administrations. The therapeutic effects of LMHO were appropriately controlled in animals, and no specific toxicity (e.g., apoptosis) was observed at the site of administration in toxicity assays (Fig. 6b, d).

In conclusion, we demonstrated how to effectively induce nano-sized saccharides and induce albumin delivery effects using LMWH, a widely used clinically polysaccharide. The optimal molecular modification of the polysaccharide LMWH through end (2-N,6-O-disulfo-D-glucosamine)-specific binding contributed to maintaining most of its therapeutic function. The introduction of hydrophobic alkyl groups induced the formation of self-assembled nanoparticles of amphiphilic LMWH molecules with a high anticoagulant effect, and these slowly migrated to albumin for sustained delivery. As a result, the combined action of the nanoparticles and the albumin delivery effect greatly increased their action time in the bloodstream, which is due to the successful effect of the slow-acting functional nanoparticles. This strategy could be adapted to the construction of other therapeutic polysaccharide molecules to improve PK properties for treatment of other diseases.

Methods

Materials

Low-molecular-weight heparins (LMWHs), including enoxaparin (purity 98%) and nadroparin, were purchased from Angene Chemical (Hong Kong). For synthesis and characterization, anhydrous dimethyl sulfoxide (DMSO, 99.5%, 276855), Benedict's reagent, anhydrous dimethylformamide (DMF, 99.8%, 227056), acetic acid (glacial, 100%, 1005-4100), albumin from human serum (purity ≥ 96%, A1653), albumin from rat serum (purity ≥ 99%, A6414), dichloromethane (DCM, 99.8%, 3030-1100), different hydrophobic alkylamines [hexylamine (C6, purity ≥ 99%, 219703), octylamine (C8, purity ≥ 99%, O5802), decylamine (C10, purity ≥ 95%, D2404), dodecylamine (C12, purity ≥ 99%, 325163), and octadecylamine (C18, ODA, purity ≥ 99%, 305391)], 1-ethyl-3-(3-dimethyl aminopropyl)carbodiimide (EDC, purity ≥ 95%, E7750), N-hydroxy succinimide (NHS, purity ≥ 98%, 130672), 2-(N-morpholino) ethane sulfonic acid monohydrate (MES, purity ≥ 99%, 69892), protamine sulfate (p4020), rhodamine B isothiocyanate (RITC, purity ≥ 90%, R105502), and sodium cyanoborohydride (087839.06) were obtained from Sigma-Aldrich. Cyanine 5.5 (Cy5.5, purity ≥ 95%, 570C0) amine was obtained from Lumiprobe (Hannover, Germany). NHS-activated agarose spin columns, sodium cyanoborohydride (purity 95%) were purchased from Thermo Fisher Scientific (Waltham, MA, USA). Fetal bovine serum (FBS) was purchased from Gibco (Milford, MA, USA). Neutral buffered formalin (10%) was purchased from HuBenTech (Damyang, Republic of Korea).

Animals

Male Sprague-Dawley rats (8 weeks, 240–260 g), male BALB/c nude mice (10 weeks, 20–25 g), and male C57BL/6 mice (8 weeks, 20–25 g) were obtained from Orient Bio (Seungnam, Republic of Korea). The rats and mice were housed in an animal facility under a 12-h light–dark cycle, with a controlled temperature of 25 ± 1 °C and humidity maintained at 50 ± 5%. Animals were euthanized using a gradual displacement measthod of CO_2 asphyxiation and terminal exsanguination while under anesthesia. All animal experiments were conducted in accordance with the standard regulations of the Institutional Animal Care and Use Committee (IACUC) at Konkuk University (Ref: no. KU22078-1, KU23255) and Seoul National University (SNU-190605-3-2).

Synthesis

We synthesized various LMWH-conjugated hydrophobic alkylamines—hexylamine (C6), octylamine (C8), decylamine (C10), dodecylamine (C12), and octadecylamine (C18)—by first completely dissolving the alkylamines in anhydrous DMF (99.8%). Subsequently, these were mixed with LMWH in distilled water. Specifically, LMWH (40 mg, 9 μmol, 1 eq.) and alkylamines (90 μmol, 10 eq.) were individually dissolved in 0.5 mL of preheated distilled water and 4 mL of anhydrous DMF at 60 °C, respectively. They were mixed with the addition of cyanoborohydride (5.6 mg, 0.09 mmol, 10 eq.) and reacted at 60 °C for 4 days. After that, 12 mL of distilled water was added to the mixture and the solution was lyophilized for 2 days. The lyophilized mixtures were purified four times to remove unconjugated alkylamines and cyanoborohydride, using precipitation in a DCM/ethanol 1:1 (v/v) solution followed by centrifugation at 1224 × *g* for 4 min each time. Residual organic solvents were evaporated using a rotary evaporator, and the final product was lyophilized for 2 days. The purified product was confirmed using TLC and RP-HPLC, utilizing a 1200 series system from Agilent Technologies (Santa Clara, CA, USA). The analysis was performed on an Eclipse Plus C18 reversed-phase column (4.6 × 150 mm, 3.5 μm), using gradient elution (water/methanol) at a flow rate of 1 mL/min and a UV-Vis detector set at 210 nm. The molecular structures of synthesized LMWH–C6, LMWH–C8, LMWH–C10, and LMWH–C12 were analyzed using a ^{1}H-500 MHz NMR (JEOL, JNM-ECZ500R/S1, Japan) at a concentration of 3 mg/600 μL of DMSO-d_6/D_2O 3:1 (v/v).

Characterization of LMHO

The specific end-group conjugation through non-enzymatic glycosylation of LMWH with alkylamine was confirmed using a two-dimensional (2D) ^{1}H-^{13}C HSQC (heteronuclear single-quantum coherence) NMR spectrometer (Bruker, 800 MHz NMR, MA, USA). LMHO was analyzed at a concentration of 20 mg/mL under the condition of DMSO-d_6/D_2O 3:1 (v/v). Additionally, the existence of aldehyde groups resulting from non-enzymatic glycosylation in LMWH was demonstrated using Benedict's reagent. Non-reducing end LMWH (NRE–LMWH), nadroparin, and LMHO were dissolved in Benedict's solution (40 mg/mL) and subjected to a low-velocity reaction with 400 rpm at 60 °C. The color change in Benedict's solution was monitored at 0, 15, 30, 60, 180, and 360-minute intervals. The relative amount of the remaining reducing end in heparin structure was measured using a calibration curve of LMWH (0–100 mg/mL) after a reaction time of 6 h.

The conjugation ratio of LMWH and ODA in LMHO was determined using a newly developed nitric oxide-based heparin degradation method[55]. LMHO was dissolved in distilled water (20 mg/200 μL). Then, aliquots of 200 μL of sodium nitrite (4 mg/40 μL) and HCl solution (1 N, 160 μL) were added to the LMHO solution. After 3 h of the subsequent reaction under light protection, the precipitate from the LMHO solution was isolated using centrifugation (15700 × *g*, 4 min) to remove residual sodium nitrite and 1 N HCl. The precipitate was resuspended in 500 μL of distilled water to remove insoluble free ODA, which was then repeated three times. The final product was lyophilized

using a freeze–dryer for 2 days and then analyzed using ^{1}H-NMR (JEOL, JNM-ECZ500R/S1, Japan), at a concentration of 1.1 mg/600 μL (DMSO-d_6). The dry weight of the powder was used to calculate the conjugation ratio of LMWH and ODA (dry powder) for LMHO.

FXa activity assay and protamine treatment

The anticoagulant activity of LMWH-conjugated alkylamines was evaluated using the COATEST anti-FXa chromogenic assay kit (Werfen, Bedford, MA). A premixture containing 100 μL of 0.3 IU of LMWH conjugates with alkylamine, 100 μL of antithrombin (AT) solution, and 800 μL of buffer solution was incubated for 3 min at 37 °C. Subsequently, 100 μL of Factor Xa (FXa) solution was added to the LMWH–AT complex solutions and incubated for another 30 s at 37 °C. Then, 200 μL of the substrate S-2222 was introduced into the system and incubated for an additional 3 min at 37 °C. To terminate the reaction, 300 μL of a 20% acetic acid solution was added. The anti-FXa activity was determined by measuring the absorbance at a wavelength of 405 nm using a microplate reader (SPECTROstar Nano Spectrometer, BMG Labtech, Germany). To evaluate the albumin binding capacity of LMWH–lipid conjugates, the conjugates were incubated with 0.02% and 0.2% albumin for an hour, followed by the above assay protocol.

The ability of LMHO to be neutralized by protamine in either buffer or rat plasma was assessed by measuring its anticoagulant activity using the COATEST anti-FXa chromogenic assay kit. The anticoagulant activity of a mixture containing 0.3 IU LMHO (2.8 μg, 1 eq.) and protamine at different ratios (1:1 or 1:5) was measured using the FXa assay protocol. In the case of animal treatment, 3 h after administering LMHO or LMWH, protamine was administered intravenously at a concentration of 25 mg/kg. Blood was collected from the rat's jugular vein at each time point (1, 2, and 3 h) and was immediately mixed with sodium citrate tribasic dihydrate solution (50 μL, 0.129 M) on ice to prepare plasma for the anti-FXa activity assay. For in vivo sustained anti-FXa activity, in addition to the first administration, subcutaneous injections of LMWH and LMHO were additionally given at subsequent time points of 60 and 132 h. The jugular vein was utilized to collect whole blood samples at intervals (12, 24, 48, 72, 96, 120, and 144 h) subsequent to the initial administration.

Molecular dynamics (MD) simulation

MD simulation of LMHO was performed using Discovery Studio software (BIOVIA, California, USA), with the molecules parameterized according to the general CHARMM force field. The MD system was solvated using the Distance-Dependent Dielectric implicit solvent model, with partial charges calculated via the Momany-Rone method. To facilitate a longer timestep, all bonds involving hydrogen atoms were constrained using the SHAKE algorithm. The Leapfrog Verlet integrator was employed for advanced dynamics integration. The heating protocol increased the system's temperature from 50 to 300 K over 4 ps, and the equilibration process, lasting 10 ps, maintained the target temperature at 300 K. For the production phase, a timestep of 600 ps was used, applying a nonbonded interaction cutoff distance of 1.4 nm for both short-range van der Waals and electrostatic interactions, determined using the spherical cutoff method. The simulation was conducted under constant temperature and pressure conditions (300 K and 1 bar) to mimic physiological environments, using NPT ensembles. After docking processes, an MD simulation of 600 ps was run following the same progression as the LMHO particle formulation. Trajectory analysis was performed during the 600 ps production phase to verify the structural and interaction efficacy of the molecules in the generated system.

Nanoparticle analysis

The particle size and zeta potential of LMHO nanoparticles were analyzed in distilled water (1 mg/mL) using dynamic light scattering (DLS; Zeta sizer Nano, Malvern Instruments, Worcestershire, UK). The nanoparticles were self-assembled by dissolving LMHO (2 mg) in 2 mL of filtered distilled water. After gently shaking the substance, the nanoparticles were sonicated at room temperature for 5 min using a JAC Ultrasonic 3010 (KODO, Republic of Korea). The stability of the LMWH–lipid nanoparticles was evaluated for 24 or 72 h by using DLS in various solutions (rat serum, DPBS, saline, DMEM, or DW). The morphology of LMHO nanoparticles was observed using transmission electron microscopy (TEM; EVO MA 10, Carl Zeiss, Germany) and field emission scanning electron microscopy (FE-SEM; MERLIN; Carl Zeiss, Germany).

Self-assembled LMHO nanoparticles were identified using the fluorescence intensity of dye-conjugated LMHO. The fluorescence intensity of the nanoparticles was visualized using a fluorescence analyzer (FOBI, CELLGENTEK, Republic of Korea) in the different concentrations of DMSO. Due to highly flexible structure of heparin, ^{1}H-NMR analysis was performed to observe the self-assembled nanoparticles, which was facilitated by the hydrophobic and hydrophilic-oriented nature of LMHO. The self-assembled nanoparticles of LMHO were investigated at various concentrations of DMSO (0–75%) using a solution of LMHO (3 mg/600 μL) with a ^{1}H-NMR 500 MHz Spectrometer (JEOL, JNM-ECZ500R/S1, Japan).

Cytotoxicity of LMHO nanoparticles

The cytotoxicity of LMHO nanoparticles was evaluated using a human-derived lung cell line (MRC-5, KCLB 10171), a canine kidney cell line (MDCK, KCLB 10034), and an adult human dermal fibroblast (HDFa, PromoCell C-12302) cell line. The cells were cultured in Dulbecco's modified Eagle's medium (DMEM) supplemented with 10% fetal bovine serum (FBS) and 1% antibiotic/antimycotic solution. The cells were seeded at a density of 1×10^4 cells/well in a 96-well plate and allowed to adhere for 1 h at 37 °C under a 5% CO_2 atmosphere. Subsequently, the cells were treated with concentration ranging from 0.01 to 100 μg/mL. After 24 h, cell viability was measured at 450 and 600 nm using the EZ-Cytox cell viability assay kit (Daeil Lab Service, Republic of Korea) and a microplate reader (SPECTROstar Nano Spectrometer, BMG Labtech, Germany). The percentage of viable cells was calculated by comparing the UV absorbance values of the samples with those of the untreated control group.

Albumin binding assay

To verify the interaction between LMHO and albumin, the size of the nanoparticles was measured at various ratios (1:1, 1:10, and 1:100, mass ratio) using dynamic light scattering (DLS; Zeta sizer Nano, Malvern Instruments). Before measurement, all materials in saline at a concentration of 0.2 mg/2 mL were gently shaken and subjected to ultrasonic treatment at room temperature for 5 min using a JAC Ultrasonic 3010 (KODO, Republic of Korea). In addition, the shape and size of nanoparticles resulting from the interaction between LMHO nanoparticles and albumin were observed using transmission electron microscopy (TEM; EVO MA 10, Carl Zeiss, Germany).

To prepare the albumin-coated column, NHS-activated agarose resin (NHS-Activated Agarose Spin Columns, Thermo Fisher Scientific, USA) (33 mg) and albumin (4 mg) were dissolved in 500 μL of distilled water. The albumin was mixed with NHS-activated agarose in the dark overnight at 4 °C. The column was then centrifuged at 1000 × *g* for a minute and washed twice with DPBS (pH 7.2, without Ca^{2+}) to remove unreacted albumin. To block any remaining active sites, 1 M Tris buffer (pH 7.4) was added to the column and mixed by shaking at 25 °C for an hour. The fluorescence intensities of LMWH–RITC and LMHO–RITC were measured in DPBS (pH 7.2, without Ca^{2+}) at a concentration of 0.8 mg/mL. A 500 μL aliquot of LMWH–RITC or LMHO–RITC was added to the albumin-coated column and left to react for an hour. The column was centrifuged at 1000 × *g* for a minute and washed four times with DPBS (pH 7.2, without Ca^{2+}). The RITC intensity of the

column was observed using a precision fluorometer (FOBI' CELLGENTEK, Republic of Korea) in the presence of 700 μL of DMSO.

For gel analysis, albumin was dissolved at a concentration of 50 μg/5 μL in DW, while LMWH–Cy5.5 and LMHO–Cy5.5 were prepared at a concentration based on Cy5.5 of 2 μg/15 μL in DW. After incubating the prepared samples on ice for an hour, they were subjected to native PAGE using a non-bromophenol blue sampling buffer. The fluorescence gel image was captured using iBright 1500 (Invitrogen; Thermo Fisher Scientific). Subsequently, the gel was fixed in a solution comprised of 50% ethanol, 10% acetic acid, and distilled water for an hour. Albumin bands within the gel were visualized by staining with 0.01% Evans blue for 20 min. The gel was then de-stained for an hour using a solution containing 50% methanol, 10% acetic acid, and distilled water. The resulting gel image was documented using iBright 1500.

Bio-layer interferometry (BLI) assay

The analysis of albumin binding kinetics was performed on the Gatorprime instrument (European Headquarters, Germany) at 35 °C under 1000 rpm conditions. After an amine-reactive sensor (Gator Probes, USA) was activated in 200 μL of distilled water for 10 min, the baseline was adjusted in 200 μL of PBS (pH 7.4) for 120 s. Activation in MES buffer (pH 5–6) with EDC/NHS solution was conducted for 400 s. Then, albumin was attached to the amine-reactive sensor in MES buffer (pH 5–6) at a concentration of 752 nM, followed by equilibration for 120 s. The binding and dissociation of albumin with LMWH or LMHO was carried out in PBS over a range of concentrations from 10 to 1.25 μM for 150 s.

In vivo pharmacokinetics of LMHO

The pharmacokinetic properties based on the level of anti-Xa activity of LMHO was investigated in the plasma of male Sprague-Dawley rats. Self-assembled LMHO nanoparticles were administered at a dose of 5 mg/kg dissolved in saline with an administration volume of 200 μL per rat (200 g), either intravenously or subcutaneously. Whole blood samples were collected from the jugular vein of the rats at predetermined time points (0.25, 0.5, 1, 2, 4, 8, 12, 24, 48, 72, and 96 h after the intravenous injection; 0.5, 1, 3, 6, 12, 24, 48, 72, and 96 h after the subcutaneous injection). The blood samples were mixed with a solution of sodium citrate tribasic dihydrate (0.129 M) and stored on ice for plasma separation. Plasma was obtained by centrifugation at 4500 × *g* for 15 min at 4 °C and stored in a −80 °C refrigerator until analyzed using an anti-FXa assay. The kinetic parameters and AUC were analyzed using non-compartmental analysis.

Endogenous albumin specificity was investigated in vivo through plasma samples procured from 8-week-old male athymic nude mice, following intravenous injection of LMWH–Cy5.5 or LMHO–Cy5.5. At an hour post-injection, the collected plasma was diluted 1:10 with distilled water and subjected to native PAGE using a non-bromophenol blue sampling buffer. Subsequently, the gel was fixed for an hour in a solution consisting of 50% ethanol, 10% acetic acid, and distilled water. Albumin bands within the gel were visualized via staining with 0.01% Evans blue for 20 min. After de-staining step, the gel image was documented using iBright 1500 (Invitrogen; Thermo Fisher Scientific).

Tail bleeding test in mice

To investigate the clotting time, LMWH or LMHO at a dose of 5 mg/kg (100 μL/25 g) was administered subcutaneously to C57BL/6 mice. The mice were anesthetized via intraperitoneal injection of 100 μL of Avertin solution (prepared by dissolving 2,2,2-tribromoethanol). A scalpel blade was used to amputate the distal 5 mm of the tail, and the amputated tail segment was immediately immersed in a beaker containing 50 mL of saline preheated to 37 °C. The onset of bleeding was observed, and the primary bleeding (coagulation) time was recorded.

In vivo biodistribution test of LMHO

LMWH–Cy5.5 or LMHO–Cy5.5 was dissolved in 100 μL of saline and then subcutaneously administered to male BALB/c nude mice (6 weeks, Orient Bio, Republic of Korea). Before administration, the fluorescence intensities of LMWH–Cy5.5 and LMHO–Cy5.5 were equalized using a high-resolution fluorescence analyzer (FOBI, CELLGENTEK, Republic of Korea). The fluorescence intensity of Cy5.5 was measured at specific time points (0, 0.5, 1, 3, 6 h, day 1, 3, 5, 8, and 14) after administration. After 1 h, and 1 and 14 days, the treated mice were euthanized, and their organs were harvested for analysis and fixed in 10% neutral buffered formalin. The fluorescence intensity of each organ was quantified using a high-resolution fluorescence analyzer (FOBI, CELLGENTEK, Republic of Korea). The fixed organ tissues were stained with hematoxylin and eosin (H&E) for histological examination. Following staining, the tissues were mounted on slides for histological observation using a multimedia digital microscope (OS-33DPM, OSUN HITECH, Republic of Korea).

Hematological analysis in rats

Hematological analysis, as a clinical pathology test, was performed on the liver and kidneys of rats treated with LMHO. Saline (control), LMWH (5 mg/kg), and LMHO (5 mg/kg) were dissolved in 200 μL of saline and administered subcutaneously. After 3 days, blood was drawn from the jugular vein of the rats to prepare serum. The levels of alanine aminotransferase (ALT), aminotransferase (AST), urea nitrogen (BUN), creatine (Crea), albumin (Alb), and the albumin/globulin ratio (A /G ratio) in the serum were measured using a biochemical analyzer (7180 Clinical Analyzer, HITACHI, Japan).

Statistical analysis

The results are presented as mean ± standard deviation (S.D.). Error bars represent the S.D. of the mean from independent samples. The statistical significance of differences between groups was analyzed using a one-way ANOVA test with post hoc testing. GraphPad Prism 9.0 (GraphPad Software Inc.) was used for all statistical analyses. Differences between groups with p-value of less than 0.05, 0.01, or 0.001 were considered statistically significant ($^{*}p < 0.05$, $^{**}p < 0.01$, $^{***}p < 0.001$).

Reporting summary

Further information on research design is available in the Nature Portfolio Reporting Summary linked to this article.

Data availability

The authors declare that all data supporting the findings of this study are available within the paper and its Supplementary Information files. Structural model of human serum albumin and heparin was deposited in protein data bank (ID:1E7H, 3IRI, 3IRL). The data that support the findings of this study are available on Figshare (https://doi.org/10.6084/m9.figshare.25719786). Also, Source data are provided with the paper.

References

1. Wang, P. et al. Heparin: an old drug for new clinical applications. *Carbohydr. Polym.* **295**, 119818 (2022).
2. Hao, C., Xu, H., Yu, L. & Zhang, L. Heparin: an essential drug for modern medicine. *Prog. Mol. Biol. Transl. Sci.* **163**, 1–19 (2019).
3. Hogwood, J., Mulloy, B., Lever, R., Gray, E. & Page, C. P. Pharmacology of heparin and related drugs: an update. *Pharmacol. Rev.* **75**, 328–379 (2023).
4. Bistervels, I. M. et al. Intermediate-dose versus low-dose low-molecular-weight heparin in pregnant and post-partum women with a history of venous thromboembolism (Highlow study): an open-label, multicentre, randomised, controlled trial. *Lancet* **400**, 1777–1787 (2022).

5. Hirsh, J. et al. Parenteral anticoagulants: American College of Chest Physicians Evidence-Based Clinical Practice Guidelines (8th Edition). *Chest* **133**, 141S–159S (2008).
6. Gray, E., Mulloy, B. & Barrowcliffe, T. W. Heparin and low-molecular-weight heparin. *J. Thromb. Haemost.* **99**, 807–818 (2008).
7. Hao, C., Sun, M. J., Wang, H. M., Zhang, L. J. & Wang, W. Low molecular weight heparins and their clinical applications. *Prog. Mol. Biol. Transl. Sci.* **163**, 21–39 (2019).
8. The Insight Partners, Low molecular weight heparin market size and growth analysis. *The Insight Partners*, TIPRE00026174, (2021).
9. Weitz, J. I. New anticoagulants for treatment of venous thromboembolism. *Arterioscler. Thromb. Vasc. Biol.* **110**, I19–I26 (2004).
10. Donat, F. et al. The pharmacokinetics of fondaparinux sodium in healthy volunteers. *Clin. Pharmacokinet.* **41**, 1–9 (2002).
11. Coyne, E. From heparin to heparin fractions and derivatives. *Semin. Thromb. Hemost.* **11**, 10–12 (1985).
12. Choay, J. et al. Structure-activity relationship in heparin: a synthetic pentasaccharide with high affinity for antithrombin III and eliciting high anti-factor Xa activity. *Biochem. Biophys. Res. Commun.* **116**, 492–499 (1983).
13. Baytas, S. N. & Linhardt, R. J. Advances in the preparation and synthesis of heparin and related products. *Drug Discov. Today* **25**, 2095–2109 (2020).
14. Bjork, I. & Lindahl, U. Mechanism of the anticoagulant action of heparin. *Mol. Cell. Biochem.* **48**, 161–182 (1982).
15. Cassinelli, G. & Naggi, A. Old and new applications of non-anticoagulant heparin. *Int. J. Cardiol.* **212**, S14–S21 (2016).
16. Lee, J. H. et al. Doxorubicin covalently conjugated heparin displays anti-cancer activity as a self-assembled nanoparticle with a low-anticoagulant effect. *Carbohydr. Polym.* **314**, 120930 (2023).
17. Plucinski, A., Lyu, Z. & Schmidt, B. V. K. J. Polysaccharide nanoparticles: from fabrication to applications. *J. Mater. Chem.* **9**, 7030–7062 (2021).
18. Lei, C. et al. Hyaluronic acid and albumin based nanoparticles for drug delivery. *J. Controll. Release* **331**, 416–433 (2021).
19. Yang, X. et al. Strategies for sustained release of heparin: a review. *Carbohydr. Polym.* **294**, 119793 (2022).
20. Pazzini, C. et al. Polymeric nanoparticles of enoxaparin as a delivery system: in vivo evaluation in normal rats and in a venous thrombosis rat model. *J. Nanosci. Nanotechnol.* **15**, 4837–4843 (2015).
21. Zeng, Y. et al. Polysaccharide-based nanomedicines for cancer immunotherapy: a review. *Bioact. Mater.* **6**, 3358–3382 (2021).
22. Karami, E., Behdani, M. & Kazemi-Lomedasht, F. Albumin nanoparticles as nanocarriers for drug delivery: Focusing on antibody and nanobody delivery and albumin-based drugs. *J. Drug Deliv. Sci. Technol.* **55**, 101471 (2020).
23. Bern, M. et al. An engineered human albumin enhances half-life and transmucosal delivery when fused to protein-based biologics. *Sci. Transl. Med.* **12**, 565 (2020).
24. Ishihara, A. et al. Prolonged residence of an albumin-IL-4 fusion protein in secondary lymphoid organs ameliorates experimental autoimmune encephalomyelitis. *Nat. Biomed. Eng.* **5**, 387–398 (2021).
25. Zaragoza, F. Non-covalent albumin ligands in FDA-approved therapeutic peptides and proteins. *J. Med. Chem.* **66**, 3656–3663 (2023).
26. Kwak, G. et al. A Trojan-Horse strategy by in situ piggybacking onto endogenous albumin for tumor-specific neutralization of oncogenic MicroRNA. *ACS Nano* **15**, 11369–11384 (2021).
27. Famta, P. et al. Albumin-hitchhiking: fostering the pharmacokinetics and anticancer therapeutics. *J. Controll. Release* **353**, 166–185 (2023).
28. Spada, A., Emami, J., Tuszynski, J. A. & Lavasanifar, A. The uniqueness of albumin as a carrier in nanodrug delivery. *Mol. Pharm.* **18**, 1862–1894 (2021).
29. Um, W. et al. A comparative study on albumin-binding molecules for targeted tumor delivery through covalent and noncovalent approach. *Bioconjugate Chem.* **30**, 3107–3118 (2019).
30. Elzoghby, A. O., Samy, W. M. & Elgindy, N. A. Albumin-based nanoparticles as potential controlled release drug delivery systems. *J. Controll. Release* **157**, 168–182 (2012).
31. Linciano, S., Moro, G., Zorzi, A. & Angelini, A. Molecular analysis and therapeutic applications of human serum albumin-fatty acid interactions. *J. Controll. Releas.* **348**, 115–126 (2022).
32. Bhattacharya, A. A., Grune, T. & Curry, S. Crystallographic analysis reveals common modes of binding of medium and long-chain fatty acids to human serum albumin. *J. Mol. Biol.* **303**, 721–732 (2000).
33. Guerrini, M. & Bisio, A. Low-molecular-weight heparins: differential characterization/physical characterization. *Handb. Exp. Pharmacol.* **207**, 127–157 (2012).
34. Park, J. et al. End-site-specific conjugation of enoxaparin and tetradeoxycholic acid using nonenzymatic glycosylation for oral delivery. *J. Med. Chem.* **59**, 10520–10529 (2016).
35. Horejs, C. From lipids to lipid nanoparticles to mRNA vaccines. *Nat. Rev. Mater.* **6**, 1075–1076 (2021).
36. Karaosmanoglu, S. et al. Carrier-free nanodrugs for safe and effective cancer treatment. *J. Controll. Release* **329**, 805–832 (2021).
37. Hirsh, J. et al. Heparin and low-molecular-weight heparin: mechanisms of action, pharmacokinetics, dosing, monitoring, efficacy, and safety. *Chest* **119**, 64S–94S (2001).
38. Linhardt, R. J. & Gunay, N. S. Production and chemical processing of low molecular weight heparins. *Semin. Thromb. Hemost.* **25**, 5–16 (1999).
39. Ernst, S., Langer, R., Cooney, C. L. & Sasisekharan, R. Enzymatic degradation of glycosaminoglycans. *Crit. Rev. Biochem. Mol. Biol.* **30**, 387–444 (1995).
40. Lau, J. et al. Discovery of the once-weekly glucagon-like peptide-1 (GLP-1) analogue semaglutide. *J. Med. Chem.* **58**, 7370–7380 (2015).
41. Liu, Q. et al. Serum albumin-peptide conjugates for simultaneous heparin binding and detection. *ACS Omega* **4**, 21891–21899 (2019).
42. Arnold, K. M. et al. Modernization of enoxaparin molecular weight determination using homogeneous standards. *Pharmaceuticals* **10**, 66 (2017).
43. Lee, S. et al. Scientific considerations in the review and approval of generic enoxaparin in the United States. *Nat. Biotechnol.* **31**, 220–226 (2013).
44. Benedict, S. R. A reagent for the detection of reducing sugars. *J. Biol. Chem.* **277**, e5 (2002).
45. Sokolowska, E., Kalaska, B., Miklosz, J. & Mogielnicki, A. The toxicology of heparin reversal with protamine: past, present and future. *Expert Opin. Drug Metab. Toxicol.* **12**, 897–909 (2016).
46. Peydayesh, M. et al. Amyloid-polysaccharide interfacial coacervates as therapeutic materials. *Nat. Commun.* **14**, 1848 (2023).
47. Meng, Q. Y. et al. Review on design strategies and considerations of polysaccharide-based smart drug delivery systems for cancer therapy. *Carbohydr. Polym.* **279**, 119013 (2022).
48. Bishop, K. J. M. Self-assembly across scales. *Nat. Mater.* **21**, 501–502 (2022).
49. Chagri, S., Ng, D. Y. W. & Weil, T. Designing bioresponsive nanomaterials for intracellular self-assembly. *Nat. Rev. Chem.* **6**, 320–338 (2022).
50. Waghule, T., Saha, R. N., Alexander, A. & Singhvi, G. Tailoring the multi-functional properties of phospholipids for simple to complex self-assemblies. *J. Controll. Release* **349**, 460–474 (2022).

51. Mulloy, B. The non-anticoagulant promise of heparin and its mimetics. *Curr. Opin. Pharmacol.* **46**, 50–54 (2019).
52. Ni, H. et al. Piperazine-derived lipid nanoparticles deliver mRNA to immune cells in vivo. *Nat. Commun.* **13**, 4766 (2022).
53. Younis, F. A. et al. Preparation, physicochemical characterization, and bioactivity evaluation of berberine-entrapped albumin nanoparticles. *Sci. Rep.* **12**, 17431 (2022).
54. Zhang, S. F. et al. Heparin-coated albumin nanoparticles for drug combination in targeting inflamed intestine. *Adv. Healthc. Mater.* **9**, 2000536 (2020).
55. Vilar, R. E. et al. Nitric oxide degradation of heparin and heparan sulphate. *Biochem. J.* **324**, 473–479 (1997).

Acknowledgements

This study was supported by Regional Innovation Strategy (RIS) through the National Research Foundation of Korea (NRF) funded by the Ministry of Education (MOE) (2021RIS-001) and the Ministry of Science and ICT (grants NRF-2020R1A2C1102831, NRF-2022R1A4A3034038, RS-2024-00394432 and RS-2024-00351420 to J.P.). This research was also supported by Young Medical Scientist Research Grant through the Daewoong Foundation (DFY2302P to J.P.). The authors are deeply grateful to Prof. Youngro Byun (SNU) and Prof. Kwangmeyung Kim (EWU) for their insightful advice.

Author contributions

Jae-Hyeon Lee and H.Lim designed and performed the experiments; Jun-Hyuck Lee, G.M. and M.S. performed animal experiments; H.Lim, H.-G.J., S.J.P. and S.-B.Y. contributed materials and analyzed the data. Jae-Hyeon Lee and S.-B.Y. collaboratively drew the scheme and figures in the manuscript using Adobe Illustrator (ver 28.4.1). Jae-Hyeon Lee, H.Lim, S.K., and J.P. co-wrote the paper. All authors discussed the results and commented on the manuscript.

Competing interests

The authors declare no competing interests.

Additional information

Supplementary information The online version contains supplementary material available at https://doi.org/10.1038/s41467-024-50819-7.

Correspondence and requests for materials should be addressed to Seho Kweon or Jooho Park.

Peer review information *Nature Communications* thanks Gloria Huerta-Angeles and the other, anonymous, reviewer(s) for their contribution to the peer review of this work. A peer review file is available.